Macedonian Journal of Chemistry and Chemical Engineering, Vol. **34**, No. 2, pp. 295–308 (2015)

MJCCA9 – 688

ISSN 1857-5552
e-ISSN 1857-5625

Received: April 11, 2014
Accepted: February 10, 2015

UDC: 544.341:546.76
Original scientific paper

KINETIC REMOVAL OF Cr^{6+} IN AQUEOUS SOLUTION BY CARBOXYMETHYL CELLULOSE-STABILIZED NANO ZERO-VALENT IRON PARTICLES

Afizah Ayob[1*], Salina Alias[2], Farrah Aini Dahlan[1], Ragunathan Santiagoo[1], Ahmad Zuhairi Abdullah[3], Tjoon Tow Teng[4]

[1]*School of Environmental Engineering, Universiti Malaysia, Perlis, Jejawi, 02600 Arau, Perlis, Malaysia*
[2]*Faculty of Civil Engineering, Universiti Teknologi Mara (UiTM) Pulau Pinang, Permatang Pauh, 13500, P. Pinang, Malaysia*
[3]*School of Chemical Engineering, Universiti Sains Malaysia, 14300 Nibong Tebal, P. Pinang, Malaysia*
[4]*School of Industrial Technology, Universiti Sains Malaysia, 11800, P. Pinang, Malaysia*

afizah@unimap.edu.my

Carboxymethyl cellulose (CMC) was used in the chemical reduction method for producing dispersible nano zero-valent iron (nZVI) particles served as reactive, mobile and convenient adsorbent. CMC-stabilized nZVI particles at CMC:Fe^{2+} = 0.0034 molar ratio were characterized using Fourier-transform infrared spectroscopy (FTIR), scanning electron microscopy (SEM), and transmission electron microscopy (TEM) assisted with probe ultrasonication dispersing tool. FTIR depicted that the CMC monomers were adsorbed onto nZVI particles primarily through carbonyl head groups via monodentate bonding. The botryoidally clusters were the predominant morphology of CMC-stabilized nZVI particles under SEM observation. Those spherical particles were evenly dispersed at sizes less than 100 nm under TEM analysis. nZVI particles stabilization with CMC (at CMC:Fe^{2+} molar ratio of 0.005) prevented the aggregation and resulted in high catalytic reactivity observed at pseudo-first order constant value, K_1 of 0.0196 min^{-1} for Cr^{6+} removal in aqueous solution. This study demonstrates that CMC-stabilized nZVI particle has the potential to become an effective agent for in situ subsurface environment remediation.

Keywords: aggregation; CMC; kinetic Cr^{6+} removal; stabilized nZVI particles; ultrasonication

КИНЕТИЧКО ОТСТРАНУВАЊЕ НА Cr^{6+} ВО ВОДЕН РАСТВОР НА НАНО-НУЛАВАЛЕНТНИ ЧЕСТИЧКИ НА ЖЕЛЕЗО СТАБИЛИЗИРАНИ СО КАРБОКСИМЕТИЛ ЦЕЛУЛОЗА

Карбокисиметил целулоза (CMC) е употребена за хемиска редукција со која се добиваат честички на дисперзивно нулавалентно железо (nZVI) кое може да послужи како реактивен, мобилен и погоден апсорбент. Со CMC-стабилизираните честички на nZVI со моларен однос CMC:Fe^{2+} = 0.0034 се карактеризирани со помош на Фуриеова трансформна инфрацрвена спектроскопија (FTIR), скенирачка електронска микроскопија (SEM) и трансмисиона електронска микроскопија (TEM) помогната со ултразвучна дисперзивна алатка. FTIR покажа дека мономерите на CMC се атсорбирани врз честичките на nZVI примарно преку карбонилните групи со монодентатно сврзување. Доминатна морфологија на CMC стабилизираните nZVI се ботриоидни кластери кои се определени со SEM. Овие сферни честички се рамномерно дисперзирани со големина помала од 100 nm како што покажува анализата со TEM. Честичките на nZVI стабилизирани со CMC (со моларен однос на CMC:Fe^{2+} од 0.005) ја спречуваат агрегацијата што резултира со висока каталитичка реактивност која е забележана кај вредноста на константа за псевдо-прв ред, K_1 од 0.0196 min^{-1} при отстранување на Cr^{6+} од водни раствори. Оваа студија покажува дека CMC стабилизираните честички на nZVI имаат потенцијал да се користат како ефикасно средство за *in situ* ремедијација на животната средина.

Клучни зборови: агрегација; CMC; кинетичкко отстранување на Cr^{6+}; стабилизирани честички на nZVI; ултрасоникација

1. INTRODUCTION

The contamination of the environment by heavy metals and the subsequent potential pollution of subsurface water are popular issues. Unlike most organic contaminants, heavy metals are transported into the environment and may encounter complex transformations that are conventionally intractable. Moreover, heavy metals persist in nature, are non-degradable, and are readily biologically detoxified [1]. Cr is categorized as one of the primary contaminants among the numerous toxic metals in the environment. Cr compounds are used in a wide variety of industrial processes such as metallurgy, chemical and refractory industries, textile dying, wood preservation, and metal electroplating processing [2, 3]. In an aqueous environment, Cr^{6+} is highly mobile and can impact large-volume aquifers, that has the potential for increased exposure and harm to human health and the environment.

The remediation of contaminated water by using nano zero-valent iron (nZVI) particles is one of the most prominent applications of nanotechnology. The most basic properties of iron, as well as the kinetic mechanisms and expected parameters, should be fully understood to consider the use of nZVI in a broader context of environment remediation. nZVI particles have great potential as redox active media because of the large specific surface area, high reactivity, and catalytic property of the particles. The metallic iron of nZVI (Fe^0) particles in an aqueous system is identified as highly capable of corrosion, which is useful in remediating contaminated water. However, the intrinsic reactivity of pure Fe^0 significantly decreases during the reaction. This phenomenon is caused by the aggregation of nZVI particles, which affects the reactive surface area and lowers particle reactivity. The phenomenon also requires the stabilization of the nZVI surface during synthesis. The stabilization technique involving the use of polar anchoring groups (e.g., –COOH, –OH, and –CO) and stabilizing hydrocarbon chains potentially inhibits the aggregation of nZVI particles through long-range steric forces and electrostatic stabilization [4, 5].

A variety of organic compounds have been examined as stabilizers, including oil-based microemulsions, surfactants, humic acid, and ionic and non-ionic polymers [5–10]. However, studies have shown that the stabilized nVZI have low stability and the particle population was poorly dispersed, which resulted in a low efficient coverage of the nZVI particles surface. Carboxymethyl cellulose (CMC) was selected considering the implications, which go beyond the simple engineering requirement for nZVI stabilization. The CMC compounds have been shown to impart enhanced particle stability because of the presence of carboxyl functional and hydroxyl groups in cellulose networks. The stabilizer-nZVI particles binding interactions, surface chemistry, and size are important in understanding the transport, reactivity and longevity, and remediation potential and fate of nZVI in the environment [9, 11].

The primary aim of the present work is to prepare a CMC-stabilized nZVI suspension through a chemical reduction method to remove Cr^{6+} in an aqueous solution, considering the physical stability and chemical reactivity of the suspension in the nZVI kinetic system. The specific objectives are to provide a tool for the preparation of a uniformly dispersed CMC-stabilized nZVI suspension and to evaluate the varying CMC:Fe^{2+} molar ratios of the suspension used for Cr^{6+} removal. The underlying particle-stabilizing mechanisms, composition, morphology, and particles size were characterized via FTIR, SEM, and TEM analyses.

2. CHEMICALS AND METHODS

2.1. *Chemicals*

All chemicals used for this experiment are of analytical or laboratory reagent grades and were used as received. Ferrous sulphate heptahydrate (> 99.9% $FeSO_4.7H_2O$) was purchased from Fisher Scientific, CMC (MW = 90 K) from Acros Organic, sodium borohydride (> 98.0% $NaBH_4$), and sodium chromate tetrahydrate (> 99.9% $Na_2CrO_4 \cdot 4H_2O$) from Sigma Aldrich.

2.2. *Synthesis of CMC-stabilized nZVI particles*

The CMC-stabilized nZVI particles were synthesized through the chemical reduction method as reported by He and Zhao [12]. The 1.0 L CMC stock solution at a concentration of 1.2% (w/w) was prepared by dissolving the CMC powder in DI water. The Fe concentration was kept constant at 2.0 g/l, and the CMC:Fe^{2+} molar ratio was fixed at 0.0034. $NaBH_4$ was added in slight (twice) excess of the stoichiometric requirement (BH_4^-:Fe^{2+} molar ratio of 2:1) and was titrated at a fast rate of 5 ml/min for a complete reaction with iron at temperatures between 10 °C and 18 °C because of the competing reaction between BH_4^- and water. The clear yellow color changed to black during the instantaneous reduction immediately after the first drop of BH_4^-. The emergence of par-

ticles was accompanied by the generation of hydrogen bubbles.

Probe ultrasonication was conducted to the CMC-stabilized nZVI suspension for around 15 min by using a probe horn sonicator at 50% amplitude power (Branson Digital Sonifier, 450). The suspension was then immediately used for the characterizations. This more powerful tool in dispersing the CMC-stabilized nZVI particle was chosen as opposed to bath sonication. Dispersing the CMC-stabilized nZVI particles by using the water bath sonicator is difficult because most of the particles remained aggregated at the bottom of the sample container and any dispersed particles quickly precipitated. The difference in dispersion is caused by the direct insertion of the ultrasonic probe in the sample and because the method used is more effective than other dispersion methods [13].

2.3. *Characterization of CMC-stabilized nZVI particles*

Fourier transform infrared (FTIR) (Nicolet i810 spectrometer, Thermo Scientific) measurements were performed to investigate the modes of interaction between CMC and the nanoparticle surface. The dried CMC-stabilized nZVI particles were mixed with potassium bromide (KBr) to obtain KBr pellets with 1.5% (w/w) nZVI particles. The sample was pressed into discs by using the Perkin-Elmer pelletizer. The FTIR spectrum of the pure 1.2% (w/w) CMC sample was used as a control spectrum. The morphology of the CMC-stabilized (2.0 g/l) and the bare nZVI particles was analyzed via field-emission scanning electron microscopy (SEM) (Leo Supra 50 VP). The structure of the CMC-stabilized nZVI particles and the non-stabilized particles were characterized using a Zeiss LIBRA 120 TEM microscope. First, the freshly prepared CMC-stabilized nZVI particles were diluted from its concentrated solution of 2.0 g/l by a dilution factor of 2 or 3 before the analysis. Bulk drops of the suspension were then placed on the carbon-coated copper grid, and filter paper was used to remove the excess sample. The residual sample attached onto the grid was then dried overnight under a N_2 flow before viewed using TEM.

2.4. *Kinetic test of Cr^{6+} removal*

The kinetic test was initiated by injecting10 mg/l to 30 mg/l of Cr^{6+} stock solution into 12 mL samples of the nZVI particle suspension, which were placed in13 ml glass vials. The solution pH was varied from 4.5 to 9.5. The concentration of the fresh nZVI suspensions was examined at a range of 0.2 g/l to 2.0 g/l. The CMC:Fe^{2+} molar ratio adjusted from 0.0017 to 0.0237, whereas the CMC concentration was kept constant at 0.9% (w/w). The injected suspension was then agitated on a rotator at a speed (ω) of 130 rpm, zero head space, a collection time of 0, 15, 30, 60, 120, 180, and 240 min, and a temperature of 30 °C. The kinetic tests were conducted at least in triplicate to ensure data quality. The control experiments were conducted at similar experimental conditions. The Cr^{6+} concentration of the supernatants was immediately filtered using a 0.45 μm (pore size) Whatman membrane filter paper. The presence of Cr^{6+} was determined using a reagent that contains an acidic buffer combined with *1,5*-diphenylcarbohydrazide, and was followed with colorimetery measurement (DR 890) at a wavelength of 540 nm.

The data were analyzed using PFO and PSO models [14] based on the following equations:

$$\log (q_e - q) = \log (q_e) - (K_1/2.303)t, \quad (1)$$

where K_1 is the rate constant of the PFO model, q is the amount of solute adsorbed on the adsorbent at time t (mg/g), and q_e is the amount of solute adsorbed on the adsorbent at the equilibrium state per unit weight of adsorbent (mg/g) for the boundary conditions $t = 0$ to > 0 ($q = 0$ to > 0).The rearranged PSO equation that follows the linear time dependence function can be represented as:

$$t/q = (1/K_2 q_e^2) + (1/q_e)t, \quad (2)$$

$$h = K_2 q_e^2, \quad (3)$$

where K_2 is the rate constant of the PSO and h is the initial sorption rate (mg/(g.min)). The rate constant (K_1 and K_2) values were derived from the slopes of the plots based on Equations (1) and (2), respectively. The h value can be determined from the intercept of the plot t/q versus t. The mass balance calculation equation was used to calculate the amount of solute adsorbed on the nZVI particles:

$$q = [(C_o - C_e) \times V]/W, \quad (4)$$

where C_0 and C_e are the initial and equilibrium concentrations of Cr^{6+} ions (mg/l) in the solution, respectively, q is the reduction capacity (mg/g), V is the volume of the solution (l), and W is the mass of the nZVI particles (g).

The solid phase morphology of the absorbed Cr^{6+} on the surface of the CMC-stabilized nZVI

particles was tested at a CMC-stabilized nZVI concentration of 1.0 g/l (CMC:Fe^{2+} = 0.0050 molar ratio) solution with a pH of 5.5 for a Cr^{6+} concentration of 30 mg/l. The solid phase morphology absorbed by Cr^{6+} onto those surface particles was characterized using SEM coupled with energy dispersive X-ray (EDX) (EDAX Inc., US).

3. RESULTS AND DISCUSSION

3.1. *Characterization of CMC-stabilized nZVI particles*

3.1.1. *FTIR*

FTIR measurements were performed to elucidate the mode of interaction between the various functional groups of the stabilizer and nZVI particles. The characteristic stretching frequencies of the pure CMC (90 K, 1.2% w/w) and the 2.0 g/l CMC-stabilized nZVI particles at a CMC:Fe^{2+} molar ratio of 0.0034 are shown in the spectra presented in Figures 1a and 1b, respectively. The assignments of the peaks obtained are summarized in Table 1. The stretching frequencies for the functional groups of CMC are expected to shift if the CMC molecules are adsorbed on the surface of the nZVI particles.

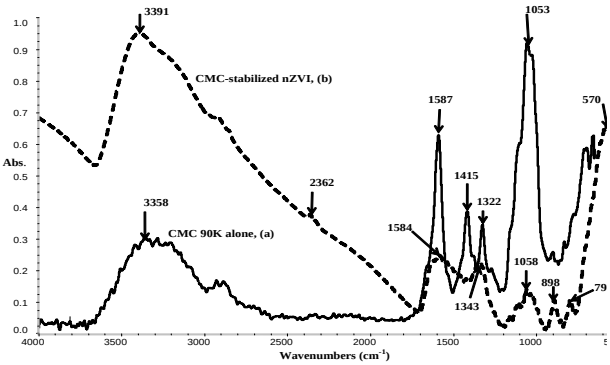

Fig. 1. FTIR spectra for (a) CMC pure 1.2% w/w, MW 90K; (b) CMC-stabilized nZVI particles

T a b l e 1

FTIR peak assignments for pure CMC and CMC-stabilized nZVI particles

Peak position (cm^{-1})		Peak assignment	References
CMC 90K -alone	CMC –stabilized nZVI		
3358	3391	Broad O–H stretch	[20]
	2362	B–OH	[27]
1587	1584	COO^- (asymmetric)	[22]
1415	–	COO^- (symmetric)	[21, 28]
1322	1343	COO^- (symmetric)	[21]
1053	–	C–O stretch	[22]
–		Fe–O	[24]
	–	Fe–O	[24]
–		Fe–O	[25]
	Δ = **241**		

The –OH stretching band notably shifts from ca. 3358 cm^{-1} for CMC (pure) to 3391 cm^{-1} for frequency (b) of the CMC-stabilized nZVI particles, which indicates the possible formation of a strong and enhanced intermolecular hydrogen bond between the CMC and nZVI particles. Given the adjusted CMC:Fe^{2+} molar ratio of 0.0034 and a high Fe concentration of 2.0 g/l, the CMC concentration is suggested to be sufficient, the effect of nucleation significant, and the amount of CMC absorbed on the particle surface enough to resist the inter-particle attractive forces. The high CMC concentration could also enhance the repulsive forces and the steric hindrance. Given the abundance of –OH groups in the CMC, this type of hydrogen bonding can be important in binding CMC to the nZVI particles. The sufficient free hydrogen bond of CMC also surrounds the exterior of the capsule and exhibits electrostatic repulsive forces composed of steric and electrostatic repulsions, which suppress particle agglomeration [15]. However, the range, efficiency, and magnitude of the electrosteric repulsion between the nZVI particles are dictated by surface concentration, extension, and charge density of the absorbed polyelectrolyte layer [16].

The complexation between a carboxylate group and a metal such as Fe^0 can take place in four types as follows: (i) monodentate chelating, (ii) bidentate chelating, (iii) bidentate bridging, and (iv) ionic interaction [17]. The first three types are illustrated in Figure 2.

The separation of the symmetric and asymmetric stretches [$\Delta\nu = \nu$ (asym) − ν (sym)] of the carboxylate group can be used to identify the bonding

mechanism compared with that of the corresponding carboxylate salts. If $\Delta\nu = 200\ cm^{-1} – 300\ cm^{-1}$, the binding is governed by a monodentate interaction. If $\Delta\nu < 110\ cm^{-1}$, the binding is governed by a bidentate chelating interaction. If $\Delta\nu = 140\ cm^{-1}$ to $190\ cm^{-1}$, the binding is governed by bidentate bridging. In this work, $\Delta\nu$ (absorbed) was determined to be $241\ cm^{-1}$ (Table 1), which indicates that covalent interaction is the primary mechanism for binding the CMC molecules to the nZVI particles and is consistent to the study of He et al. [18]. Authors have reported that the main binding mechanism of the nZVI-CMC complex is a bidentate bridging configuration [19], which may be attributed to the differences in the suspension pH and the ion strength used by the said authors.

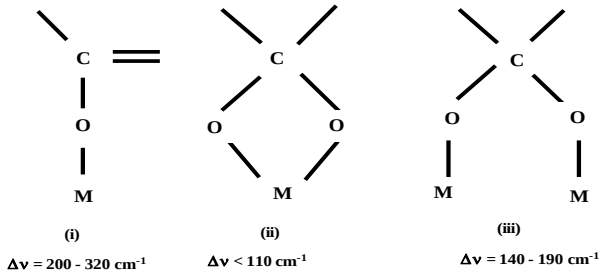

Fig. 2. Modes of metal-carboxylate complexation (a) monodentate chelating; (b) bidentate chelating, and (iii) bidentate bridging. $\Delta\nu$ is the separation frequencies between the symmetric and asymmetric stretches of the carboxylate group.
M is metal of Fe.

The carboxylate functional group found in the CMC coupled strongly with the Fe^{2+} ions in the precursor solution ($FeSO_4 \cdot 7H_2O$). This functional group was then dispersed with Fe^{2+} and promptly nucleated after borohydride reduction throughout the CMC monomers [18]. The sharp strong band at ca. $1587\ cm^{-1}$ in the CMC spectrum alone (Fig. 1a) was attributed to carbonyl group stretching. The anionic polyelectrolytes, CMC, underwent protonation through the carboxylic group to reduce intra-layer density and were then adsorbed onto the iron oxide surfaces, which extended the chain conformation. This claim was supported by Phenrat et al. [16], who studied the dispersion of nZVI particles by ionic polyelectrolyte. The small peak at $2362\ cm^{-1}$ could also be caused by the bonded B–OH spectrum, whereas B–O stretching occurs from the $700\ cm^{-1}$ to $1000\ cm^{-1}$ region [20], which indicates the presence of a free boron element in the CMC-stabilized nZVI particles because of the high BH_4^-:Fe^{2+} molar ratio applied during the reduction process.

The region from $1200\ cm^{-1}$ to $1350\ cm^{-1}$ was assigned as the progressional band because of the effect of the ultrasonication dispersion tool (Fig. 1b). The obtained region is consistent with the study by Kataby et al. [21] where carboxylic acids are coated on amorphous iron nanoparticles. In this region, the appearance of the zigzag band structure indicates a fully extended O–H chain with a transconfigurational structure, and that the carboxylic groups were strongly attached to the nanoparticles. The carboxylate groups can also bind differently onto each metal during the self-assembly of the monolayer coating of the carboxylic acids on the iron amorphous surface. The molecules were presumably symmetrically bonded at an angle on the surface.

The typical Fe–O bond characteristic was visible at lower wavenumbers between 800 and $400\ cm^{-1}$ [22]. An investigation of these (Fe–O) bands was first reported by Waldron [23] at ca. 575 and $375\ cm^{-1}$ for the metal ion bond deformation. In the present work, the strong interaction between the nZVI particles and polyelectrolytes subsequently increased the surface bond constant, altered the electron density, and rearranged nonlocalized electrons. The absorption frequency of the Fe–O bond simultaneously shifted to ca. 898 and $797\ cm^{-1}$. However, the peak at $570\ cm^{-1}$ shifted to a higher intensity possibly because of the stronger Fe–O bond (Figure 1b). A similar characteristic absorption band was observed by Lin et al. [24] during the preparation of a stabilized superparamagnetic ferrofluid.

The primary physisorption mechanism of the coated CMC-nZVI consequently occurred through both electrostatic and strong long-range repulsive forces, which prevented particle aggregation and deposition and ensured the mobility of the nanomaterials in the subsurface environment [4, 19]. However, given the small semi-crystalline-amorphous size of the nZVI particles, the repulsive energy barrier of the nZVI particles for opposing aggregation and deposition may be weaker compared with that of the micron-scale particles of the same surface. The presence of excess free CMC (based on CMC:Fe^{2+} molar ratio = 0.0034) that were unabsorbed onto the nZVI particle surface apparently also affected the stabilization of the nZVI suspension.

3.1.2. *SEM*

SEM analysis was performed for the non- and CMC-stabilized nZVI particles (Fig. 3) to further aid the identification of the magnified images. The significant effects on the surface texture for both particle types were visually distinguishable. No specific shapes or patterns for any of the individual particles were observed for the non-stabilized nZVI particles (Figs. 3a and 3b). However, the obtained particles appeared to have a

densely packed morphology at the sub-micron scale larger than 5 μm (Fig. 3b). The observed morphology of these bare particles without the effect of probe ultrasonication dispersion can maximize the coordination number, minimize surface free energy, and minimize the surface to area ratio of the particles. All of these particles were aggregated because of the magnetic properties and the tendency to remain in the most thermodynamically favorable state of both particles [19].

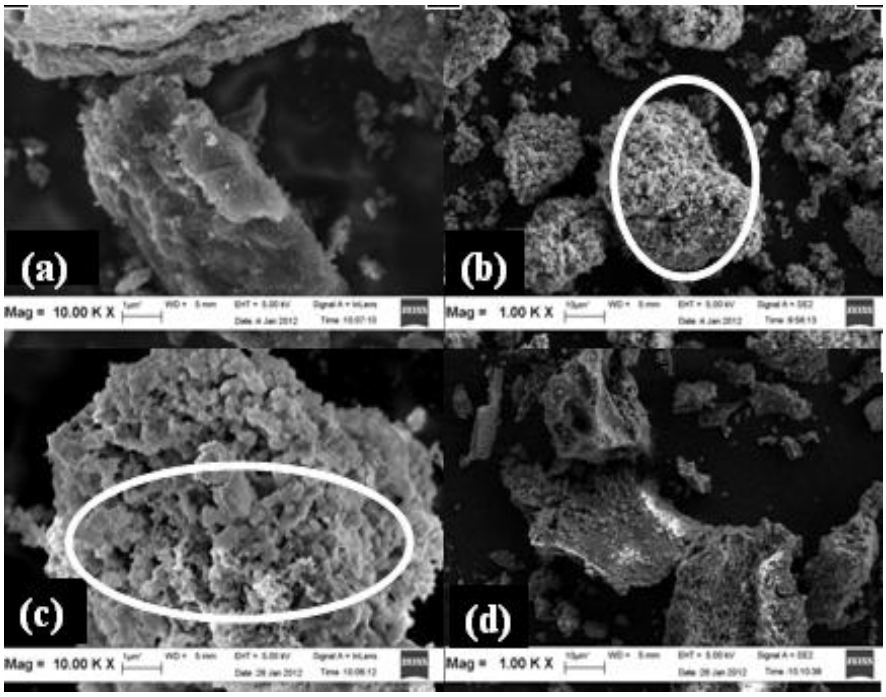

Fig. 3. SEM morphology of (a) long rectangular shape, (b) bulky bare of non-stabilized nZVI, (c) surface coated by CMC, (d) euhedral shape of CMC-stabilized nZVI particles

The nZVI particle surfaces were obviously coated with a uniform white/clear CMC stabilizer with some CMC possibly between the dispersed particles (Fig. 3c). The shape of the CMC-stabilized nZVI particles was euhedral, irregular, and square (Figure 3d). Botryoidally clusters were the predominant morphology of the CMC-stabilized nZVI particles, where the particle was continuous and had rounded packing (Fig. 3c). Many finer CMC-stabilized nZVI particles with sizes less than 10 nm were observed to pack together into larger particles with sizes of 30 nm to 50 nm. The smaller primary nZVI particles that were energetically unstable assembled themselves into larger spherical nZVI particles because of Ostwald ripening [19]. The excess CMC (CMC:Fe^{2+} molar ratio = 0.0034) that were confirmed by the extended –OH chains and the carboxylate groups that were coated (in FTIR analysis) on the nZVI were possibly caused the abundant defects of the CMC-stabilized nZVI particles (Fig. 3b).

3.1.3. *TEM*

Transmission electron microscopy (TEM) analysis was performed to investigate the size, shape, and morphology of the non- and CMC-stabilized nZVI particles (Fig. 4). The non-stabilized nZVI particles appeared to be fused to one another possibly because of the strong magnetic dipole–dipole attractions between the non-stabilized individual nZVI particles (Fig. 4a). The CMC-stabilized nZVI particles at a CMC:Fe^{2+} molar ratio of 0.0034 were polydispersed with no aggregation observed in the solution (Fig. 4b). The CMC-stabilized nZVI particles were largely spherical, and the size of almost all the individual particles was less than 100 nm. This observation could be caused by the rapid nucleation and crystal growth during the titration of a high amount of BH_4^- in the reduction process. The CMC-complexed Fe^{2+} ions were then reduced to elemental Fe. However, He and Zhao [26] observed much larger aggregates at a lower CMC:Fe^{2+} molar ratio of 0.0062 with a 0.1 g/l concentration of Fe. CMC-stabilized particles at a CMC:Fe^{2+} molar ratio of 0.0005 (CMC 0.7 degree of substitution) with a diameter of less than 10 nm was observed via TEM by Greenlee and Hooker [29], which indicates that an optimum CMC:Fe^{2+} molar ratio is required to achieve particle stabilization.

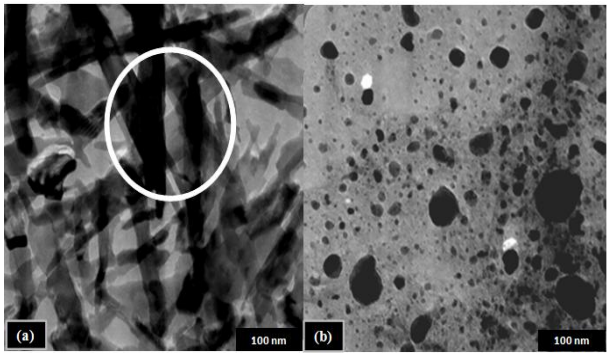

Fig. 4. TEM morphology of (a) non-stabilized nZVI particle fused to each other; (b) well and small dispersed of CMC-stabilized nZVI particles of 2.0 g/l concentration suspension

The sizes of the rectangular and/or irregularly shaped particles were generally larger than those of the small round particles (Fig. 4b). This variation was caused by the forces that hinder crystalline nZVI core formation. Therefore, the small radii of the nZVI particles and the curvature of the oxide shell contributed to the formation of those irregular shapes. The reaction of the residual boron (caused by an excess amount of BH_4^-) in the oxide layer partly caused defects in the formation of the oxide layer. Free boron constituents (B–O or B–OH) were detected via FTIR analysis before the reaction. This unique configuration protected the core iron against further oxidation and provided a means for mass and charge transport.

The obtained small CMC-stabilized nZVI particles with sizes less than 20 nm were attributed to the probe ultrasonication tool (50% amplitude power; Fig. 4b). This technique separated the CMC-stabilized nZVI particles into smaller monomers instead of an aggregated form, which extended the settling time. Increasing the time period of probe ultrasonication (more than 15 min) of the CMC-stabilized nZVI particles dispersion reduced the aggregate size. The acoustic waves imparted through ultrasonication effectively disperse those particles because transient cavitation and acoustic streaming can possibly redefine the shape, structure, and surface morphology of the CMC-stabilized nZVI particles [28]. However, the dispersion tool was unable to break the CMC-stabilized nZVI particles down to the primary diameter because of the possible aggregation of the particle during extended storage periods or synthesis or because pre-existing aggregates could not be dispersed through sonication. This reason could explain the existence of larger particles at around 60 nm to 80 nm (Fig. 4b). Excess amounts of the stabilizer (carboxylate molecules) in the solution possibly caused the different sizes and morphologies [19] of the CMC-stabilized nZVI particles (CMC:Fe^{2+} = 0.0034 molar ratio) as detected earlier through FTIR analysis. Therefore, the monomer networks of the CMC structure functioned as a colloidal trap to stabilize the dispersion of the nZVI particles.

3.2. *Kinetic test of Cr^{6+} removal*

3.2.1. *Effect of adsorbent types*

This study focused on gaining mechanistic insights into the chemical reduction of Cr^{6+} in an aqueous solution by using 1.0 g/l CMC-stabilized nZVI particles (CMC:Fe^{2+} molar ratio = 0.0050) and a related kinetics system. The adsorption mechanism and reduction rate that incorporated the effects of the various adsorbent types, solution pH, CMC-stabilized nZVI particles concentration, and initial Cr^{6+} concentrations were evaluated by testing the applicability of PFO and PSO kinetic models. The kinetic parameters were estimated through linear curve fitting derived using Equations (1) and (2). The conformity between the experimental data and the predicted kinetic model was based on the correlation coefficient (adjusted R^2 value; Table 2). In this case, the adjusted R^2 value was calculated using the square of the sample correlation coefficient once the data was fitted to the linear regression. The adjusted R^2 value is the validity between the outcomes and the predicted value.

In this study, different removal pathways were involved when a stabilizer was introduced into the system. Complicated kinetic behavior was observed. The suggested kinetic steps included the rapid corrosion of CMC-stabilized nZVI particles through adsorption by the particles surface followed by a redox reaction under the existence of Fe^0, which allowed co-precipitation to take place. By contrast, a primary redox reaction of Fe^0 followed by more rapid physical or chemical adsorptions was suggested by Geng et al. [29] in their study where chitosan-coated iron nanoparticles were used to remove Cr^{6+}. The overall kinetic mechanisms possibly overlaid different reactions or/with different kinetics orders [30]. The PFO model (Fig. 5) in the present study was suitable in removing Cr^{6+} in an aqueous solution based on the adjusted R^2 values for the four different factors (adsorbent types, solution pH, CMC-stabilized nZVI particles concentration, and Cr^{6+} concentrations; Table 2). In the first effect of the different absorbent types, the adjusted R^2 values for the PFO model range from 0.0623 to 0.9706 (Fig. 5a), which is different from the poor correlation coefficients of PSO (0.0090 to 0.9358). Previous investigations on Cr^{6+} removal in other nZVI particle systems were also reported as PFO [31, 32].

T a b l e 2

PFO kinetics model for Cr^{6+} removal in contaminated aqueous

Effects	Adjusted R^2	K_1 (min^{-1})
Adsorbent types		
Non-stabilized nZVI (pH 5.5, 1.0 g/l concentration, 10 mg/l Cr^{6+} concentration)	0.9172	7.3696E-3
CMC-stabilized nZVI (CMC:Fe^{2+} molar ratio = 0.0050, pH 5.5, 1.0 g/l concentration, 10 mg/L Cr^{6+} concentration)	0.9706	0.0196
Commercial nZVI	0.0623	3.6848E-3
DI water	0.8031	0.0157
Solution pH		
4.5	0.9795	0.0193
7.5	0.9042	9.6726E-3
9.5	0.9838	0.0124
nZVI particles concentration (g/L)		
0.2 (CMC:Fe^{2+} molar ratio = 0.0237)	0.9070	0.0104
0.8 (CMC:Fe^{2+} molar ratio = 0.0058)	0.9858	0.0113
2.0 (CMC:Fe^{2+} molar ratio = 0.0017)	0.9828	0.0216
Concentrations of Cr^{6+} (mg/L)		
7	0.8894	0.0281
20	0.9777	0.0131
30	0.9068	0.0127

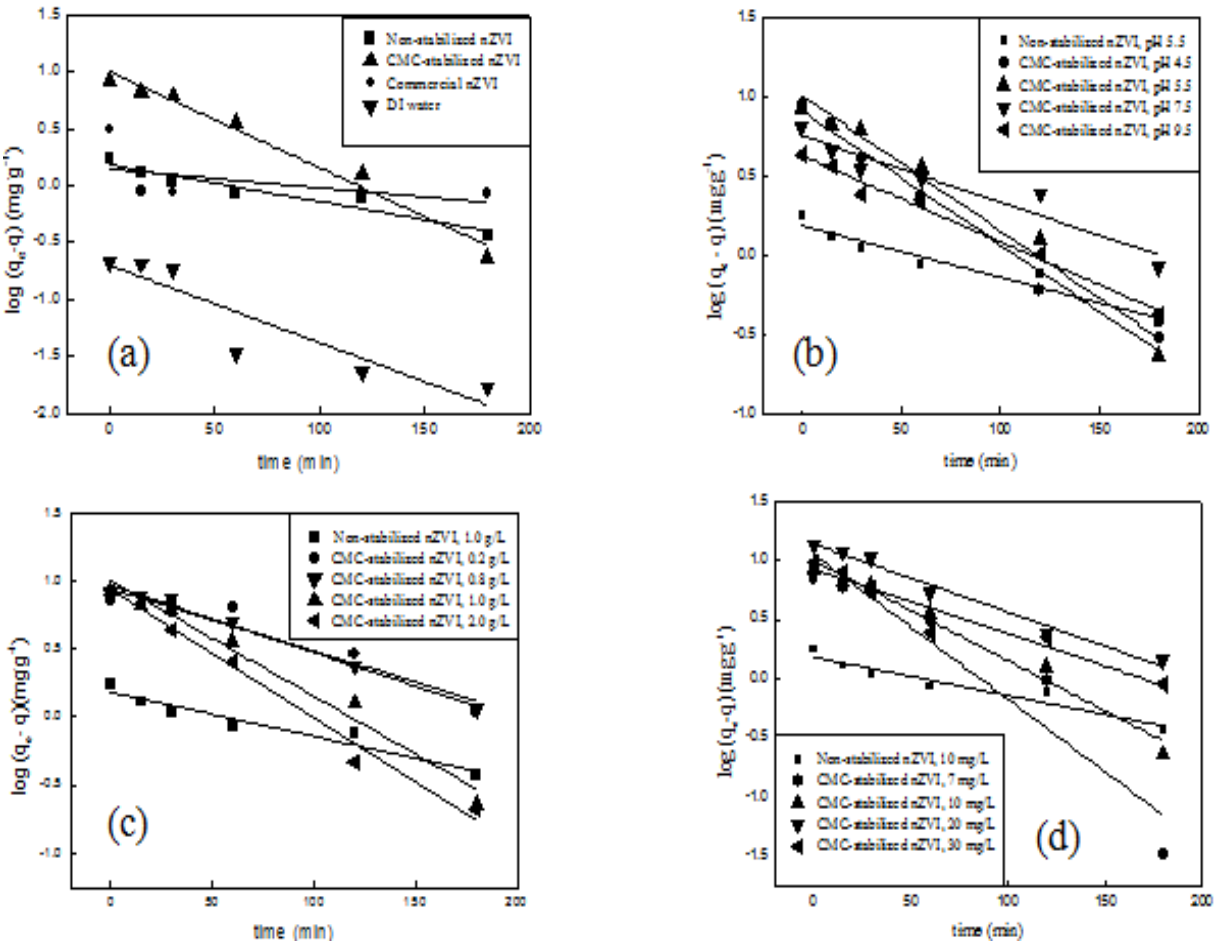

Fig. 5. Factor influencing the PFO kinetic model of Cr^{6+} removal (a) adsorbent types; (b) pH solution; (c) CMC-stabilized nZVI particles concentration; (d) Cr^{6+} concentrations, experimental condition conducted at similar agitation duration = 240 min, ω = 130 rpm, and T = 30 °C.

The FTIR results of the present study indicate that the CMC molecules were absorbed onto the nZVI particle surface through the COO^- and –OH groups (Fig. 1). Only a fraction of the COO^- and –OH groups in CMC were presumably involved in the interaction with the nZVI particles, which lead to the availability of more fresh sites for further reaction, based on CMC stereochemistry and the thermodynamics of the system. The sorption of the CMC monomers from a mass transfer standpoint was generated in an unstrained and assembled layer of CMC molecules on the nZVI particles [33]. This phenomenon decreased the Cr^{6+} mass transfer resistance to the reactive sites of the CMC-stabilized nZVI particles. The CMC-stabilized nZVI particles at a CMC:Fe^{2+} molar ratio of 0.0050 were sufficient as the adsorbent for this case. The sorption of the CMC monomers enhanced the removal reaction rate compared with that of the non-stabilized nZVI counterpart.

The recorded Cr^{6+} removal kinetic rates values K_1 were 7.3696E-3, 0.0196, 3.6848E-3, and 0.0157 min^{-1} for the non-stabilized nZVI, CMC-stabilized nZVI particles, commercial nZVI, and DI water, respectively (Table 2). Therefore, the CMC-stabilized nZVI particles at the same concentration (1.0 g/l) removed Cr^{6+} approximately three times faster than the non-stabilized nZVI particles. The K_1 value obtained in this study was higher than the previously reported 1.3330E-3 min^{-1}, where the CMC-stabilized nZVI particles used had a concentration of 0.0810 g/l and with an initial Cr^{6+} concentration of 34 mg/l [34]. The CMC-stabilized nZVI suspension concentration in this study was ~12 times greater and the initial Cr^{6+} concentration of 10 mg/l was 3.4 times lower than those used by Xu and Zhao [34]. This observation could be caused by the increase in the active sites by using a higher concentration of the CMC-stabilized nZVI suspension. The small particles obtained after probe ultrasonication dispersion can regulate the redox chemistry in the solution and enhance the removal rate constant K_1 values.

CMC can hinder the formation of Fe-Cr precipitate when the stabilizer is introduced into the system because of the coordination capability CMC. This co-precipitate would reduce the electron transfer from Fe^0 to metal ions, which eliminated the removal of Cr^{6+}. However, stabilizer monomers, such as –COO and –OH groups, on the bulky CMC-stabilized nZVI surface function as covalent ligands that coordinate with the transition metals (Cr^{6+}), which further increases the K_1 values. The behavior of the ligand bonding was observed beforehand via FTIR analysis. The overall removal mechanism was apparently more complicated than a simple chemical one.

3.2.2. *Effects of solution pH*

The kinetics mechanism that is affected by the solution pH was evaluated using PFO model (Fig. 5b). The correlation coefficient of the best fitted PFO model was slightly higher with the adjusted R^2 values from 0.9042 to 0.9838 compared with 0.8893 to 0.9587 of PSO (Table 2). The measured K_1 values were 0.0193, 0.0196, 9.6726E-3, and 0.0124 min^{-1} for the CMC-stabilized nZVI particles (1.0 g/l concentration, CMC: Fe^{2+} = 0.0050 molar ratio) at pH values of 4.5, 5.5, 7.5, and 9.5, respectively, for Cr^{6+} removal at a concentration of 10 mg/L. These K_1 values revealed the existence of a strong correlation between the CMC-stabilized nZVI corrosion and Cr^{6+} removal.

A change in the pH media significantly changes the stabilizer charges. In such a case, more protons accumulate on the CMC monomer in an acidic medium, which changes to more positively charged CMC-stabilized nZVI particles. Therefore, the electrostatic attraction between the positively charged CMC-stabilized nZVI particles and the negatively charged chromate anion accelerate Cr^{6+} adsorption and kinetically enhance the Cr^{6+} to Cr^{3+} reduction rate. However, pH proton supplies became scarce at higher solution. The rate-controlling step governed by the CMC-stabilized nZVI corrosion gradually shifted and relatively decreased the K_1 values as shown in a solution with pH values of 7.5 and 9.5 (Fig. 5b).

More hydrogen gas was generated through the CMC-stabilized nZVI particles corrosion reaction at a lower solution pH. The proton (H^+) accepts the electrons released by Fe^0 following Equation (5):

$$Fe^0_{(s)} + 2H^+_{(aq)} \rightarrow Fe^{2+}_{(aq)} + H_{2(g)}, \qquad (5)$$

In this case, the H_2 bubbles were visualized inside the vial at the nZVI-suspension interface, especially at the beginning of the experiment. The H_2 bubbles then disassociated to form atomic H, which significantly affects the kinetic rate of Cr^{6+}. The formation of passivated surface layers may presumably be difficult at a low solution pH (lower than 3.0) because of the precipitations of metal hydroxides and carbonates on the iron surface [31]. The CMC-stabilized nZVI particles also tend to utilize H_2 rather than that of the Cr^{6+} reduction at a low solution pH. The rapid H_2 evolution and nZVI particle consumption affected the relatively shortened reactive lifetime of the CMC-stabilized nZVI. Particle efficiency also deteriorated because of the decrease in solution pH. No attempt was made in this present study to eliminate the residual H_2 inter-

ference during the preparation of the CMC-stabilized nZVI particle, which can slightly affect the Cr^{6+} removal process. Cr^{6+} reduction with CMC-stabilized nZVI particles and subsequent Cr^{3+} oxyhydride precipitation were also developed using Equation (6):

$$Cr_2O_7^{2-}{}_{(aq)} + 3Fe^0{}_{(aq)} + 14H^+{}_{(aq)} \rightarrow 2Cr^{3+}{}_{(aq)} + 3Fe^{3+}{}_{(aq)} + 7H_2O, \quad (6)$$

A parallel passivation reaction developed during the Fe-Cr^{6+} proximity. This phase was considered as the nZVI surface passivation or the "active site" as the reduction rate decreased with contact time. The CMC-stabilized nZVI (Fe^0) changed to Fe^{3+}-Cr^{3+} oxyhydroxide with low electrical conductivity at this point, which prevents the electron flow passage from Fe^0 to Cr^{6+}. However, the mixed Fe^{3+}-Cr^{3+} formation solubility was also lower and decreased the kinetic reaction at a lower pH solution. Cr^{6+} removal can be influenced by iron geochemistry (dissolution and precipitation) despite the effects of H^+ generation [35].

3.2.3. *Effects of CMC-stabilized nZVI particles concentration*

The PFO kinetic rate model plots of Cr^{6+} removal at different CMC-stabilized nZVI concentrations of 0.2 g/l to 2.0 g/l (CMC:Fe^{2+} molar ratio from 0.0017 to 0.0237) are depicted in Figure 5c. Higher adjusted R^2 values of the PFO model were obtained compared with the very poor correlation coefficient of PSO (values not shown). The Cr^{6+} removal kinetic rates increased with increasing CMC-stabilized nZVI suspension concentration. The measured K_1 values of the Cr^{6+} removal rates increased from 0.0104, 0.0140, 0.0196, and 0.0216 min^{-1} for the 0.2, 0.8, 1.0, and, 2.0 g/l concentrations, respectively, of the CMC-stabilized nZVI particles (Table 2). The presence of CMC yielded stable nanoparticles and considerably enhanced the reactive surfaces, which caused a higher K_1 values.

In this study, the molar ratio of CMC:Fe^{2+} proportionally increased in kinetic reactivity (trend of 2.0 g/l concentration; Fig. 5c). However, CMC molecules could cover the formation of a significant number of reactive sites as a compact coating on the surface at a high molar ratio, which adversely affects the accessibility of the target compounds to reaction sites and result in a decrease in the reactivity rate. Therefore, optimizing the CMC:Fe^{2+} molar ratio during synthesis could enhance the performance of the CMC-stabilized nZVI particles.

3.2.4. *Effects of Cr^{6+} concentrations*

The PFO plot of the Cr^{6+} removal kinetic rates at various initial Cr^{6+} concentrations are shown in Figure 5d. The kinetic rate constant of Cr^{6+} removal decreased with increasing initial Cr^{6+} concentration (Table 2). The initial Cr^{6+} concentration obviously had a major influence in the Cr^{6+} removal process. The K_1 values were 0.0281, 0.0196, 0.0131, and 0.0127 min^{-1} for initial Cr^{6+} concentrations of 7, 10, 20, and 30 mg/l, respectively, of the CMC-stabilized nZVI particles (1.0 g/l concentration, CMC:Fe^{2+} = 0.0050 molar ratio).

Cr^{6+} is a strong oxidant compared with the well-known passivator of Fe [36]. More CMC-stabilized nZVI particles can be theoretically oxidized and passivated with the continuity of the reaction because more oxidants are attached to the nZVI particle vicinity, which is attributed to the decrease in activities and K_1 values of the oxidants. Cr^{6+} was more likely absorbed to the CMC-stabilized nZVI particle. Primary oxidation of Fe^0 to Fe^{3+} followed. Cr^{6+} was reduced to Cr^{3+} at the same time to complete the removal process. A thin layer of Fe^{2+}-Cr^{3+} hydroxides developed when both elements were in proximity, which increased electron transfer resistance from the CMC-stabilized nZVI particles to Cr^{6+} through electrochemical pathways. This result retarded the removal mechanism and lowered K_1 values.

All PFO kinetic trends in the case of adsorption were judged from four different effects (Fig. 5) via regression coefficient lines that did not cross the origin, which indicates that physical adsorption is essential in Cr^{6+} removal. For example, this result can be seen in a solution with pH values of 5.5, 4.5, and 9.5 (Fig. 5b). More complicated physical and chemical adsorptions can lead to the overall mechanism of Cr^{6+} dissipation if the lines intercepted the origin.

Predicting the rate at which adsorption takes place for nZVI system is probably the most important factor in adsorption system design with the absorbate residence time and the reaction dimension controlled by the kinetics of the system. The variation of the experimental data (q_e) and the calculated data (q_c) for the adsorption of Cr^{6+} associated with the PFO kinetic rate constant is shown in Table 3. The q_c values were much lower than the amount absorbed values based on experimental results, which can be seen for all four effects at various adsorbent types, solution pH, CMC-stabilized nZVI particles concentration, and Cr^{6+} concentrations.

T a b l e 3

Experimental (q_e) and calculated (q_c) data for the adsorption of Cr^{6+} associated respectively with PFO rate equations

Effects	q_e	q_c
Adsorbent types	1.750	1.197
	8.379	2.710
	3.111	1.152
	0.211	0.495
Solution pH	8.780	2.462
	8.379	2.711
	6.320	2.110
	4.308	1.862
nZVI particles concentration (g/l)	7.070	2.556
	8.379	2.711
	8.140	2.625
	8.659	2.552
Concentration of Cr^{6+} (mg/l)	6.899	2.839
	8.379	2.711
	13.500	3.114
	9.540	2.518

However, the difference is too large between the experimental data and the theoretical data for the effect of the Cr^{6+} concentrations in this nZVI system. The variation can be seen at Cr^{6+} concentrations of 20 mg/l and 30 mg/l with a high amount absorbed at 13.50 mg/g and 9.54 mg/g, respectively, based on experimental results. This result shows that the CMC-stabilized nZVI particles have a high adsorptive capacity to Cr^{6+} in contaminated water.

3.2.5. *Solid phase characterization*

The surface analysis of Cr^{6+} adsorbed onto the surface of the CMC-stabilized nZVI particles were performed via SEM after 240 min of the removal process (Fig. 6). The SEM characterization was performed to understand further the metal uptake mechanisms and the determination of the parameters that govern the long-term treatment process. The surface layers of the raw CMC-stabilized nZVI particles were coated with CMC stabilizers (Fig. 6a). The SEM micrographs illustrate the pronounced corrosion effect and the formation of an oxide layer on the CMC-stabilized nZVI surface after Cr^{6+} removal (Fig. 6b). The deposited flake-like ions and the rough surfaces were visually discernible after the initialization of the adsorption, redox, and co-precipitation processes [36].

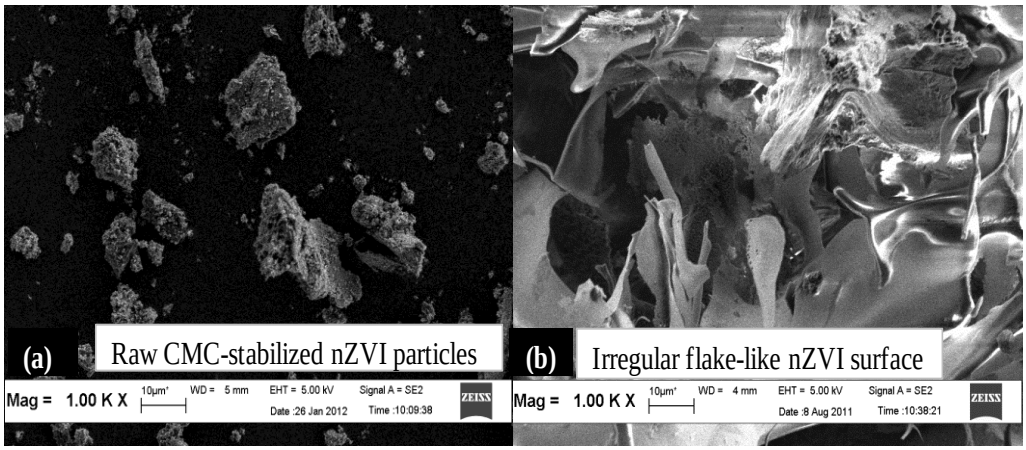

Fig. 6. SEM micrographs of (a) CMC-stabilized nZVI particles before reaction; (b) surface corrosion of CMC-stabilized nZVI particles after Cr^{6+} absorbed.

The sizes of the CMC-stabilized nZVI particles prominently increased after the reaction with Cr^{6+}, which confirms the co-precipitation of Cr^{3+}-Fe^{3+} on the spent surface that spontaneously occurred because of the redox reaction [32]. Rough and exhausted surface layers formed after the reaction because the precipitation of the metal hydroxides on the CMC-stabilized nZVI reflects the possible removal mechanism of Cr^{6+} (Fig. 6b). A conclusion can be drawn when the information from the SEM images on the spent surface is combined with the detection metal ions in the solution, the reduction of Cr^{6+} to Cr^{3+} and the oxidation of Fe^0 to Fe^{3+} preceded synergistically. This result occurred when the diffusion pathway and the reaction reached the completion time that determined the removal rate of Cr^{6+} [29].

The EDX spectra of randomly selected spots in the fresh CMC-stabilized nZVI particles and on the spent nZVI surface (Fig. 7) were obtained to evaluate the presence of the corresponding element after the reaction with Cr^{6+}. The composition of the

particles was inferred from the SEM images and the amplitudes of various EDX peaks. The specimen contained C, O, Na, and S from left to right, which are attributed to the stabilizer (CMC) and precursor ($FeSO_4.7H_2O$) compounds. The spectra show that the fresh CMC-stabilized nZVI particles (CMC:Fe^{2+} = 0.0050 molar ratio) contained 11.01% Fe, 27.99% O, 25.52% C, 20.13% Na, and 15.53% S (Fig. 7a). The elements O and C are significantly higher based on the CMC:Fe^{2+} molar ratio.

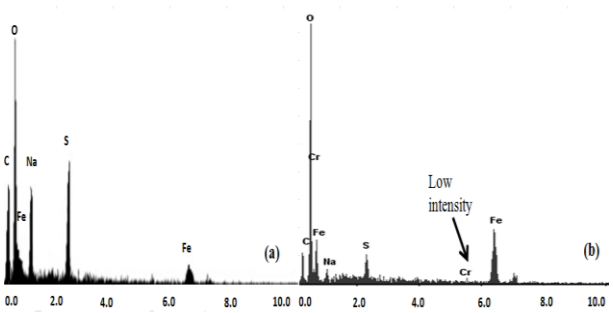

Fig. 7. EXD mapping of (a) CMC-stabilized nZVI particles before reaction, (b) Cr^{6+} absorbed onto 1.0 g/l CMC-stabilized nZVI particles at CMC:Fe^{2+} = 0.005 molar ratio.

The amount of Fe increased to 43.44%, and O, C, Na, and S were recorded to be 33.21%, 17.05%, 2.03%, and 3.68%, respectively, after the reaction with Cr^{6+} (Fig. 7b). The Cr signal appeared low (0.58%) from 5 keV to 6 keV, which indicates that Cr was deposited onto the exhausted CMC-stabilized nZVI particles. The low Cr intensity can also be caused by the Cr^{6+} adsorption on the nZVI surface. Previous reports provided evidence of scrap iron observed on nanoparticle surfaces after Cr^{6+} reduction [3]. A higher recorded Fe composition at 43.44% for Cr^{6+} adsorption test is expected because of the oxidation and corrosion effect of CMC-stabilized nZVI particles in an aqueous medium. The higher Fe content could also be caused by the original molar ratio of CMC:Fe^{2+} at 0.0050. The iron oxides or hydroxides and some co-precipitates of Fe-Cr on the surface of the CMC-stabilized nZVI further increased the percentage of the Fe element. The higher Fe composition obtained after Cr^{6+} reaction could also be attributed to the high reduction potentials (E^{θ} = 1.36 V) at which the direct electrons transfer from the nZVI particle were faster for a more positive cation such as Cr^{6+}.

4. CONCLUSIONS

The CMC-stabilized nZVI particles (CMC:Fe^{2+} = 0.0034 molar ratio) displayed much less agglomeration but high catalytic removal power than those prepared without a stabilizer. All characterization findings were sufficient to explain quantitatively the ultrasonication procedure effects of the disaggregation of the CMC-stabilized nZVI particles. The characterization contributes much insight into the synthesizing process, which requires an understanding of the dispersing effects via both chemical and physical techniques. Stabilizing the nZVI particles with CMC with the assistance of an ultrasonic probe revealed the chemical interaction, reduced particle size, and widely varied surface characteristics. Herein, the CMC-stabilized nZVI particles exhibited higher removal efficiency followed the PFO model at constant value, K_1 of 0.0196 min^{-1} for removal of 10 mg/l Cr^{6+} concentration in aqueous media. These characteristics of CMC-stabilized nZVI particles could later predict overall mobility, reactivity, and transport in contaminated water mediums for in situ remediation of Cr^{6+}.

Acknowledgement. We gratefully acknowledge the funding from PRGS (USM) grant no. 1001/PTEKIND/842002.

REFERENCES

[1] A. Ahmad, M. Rafatullah, O, Sulaiman, M. H. Ibrahim, Y. Y. Chii, B. M. Siddique, Removal of Cu(II) and Pb(II) ions from aqueous solutions by adsorption on sawdust of Meranti wood, *Desalination*, **247**, 636–646 (2009).

[2] M. Owlad, A. Kheireddine, W. A. W. Daud, S. Baroutian, Removal of hexavalent chromium contaminated water and wastewater: a review, *Water Air Soil Poll.*, **200**, 59–77 (2009).

[3] M. Gheju, I. Balcu, Removal of chromium from Cr (VI) polluted wastewaters by reduction with scrap iron and subsequent precipitation of resulted cations, *J. Hazard. Mater.*, **196**, 131–138 (2011).

[4] N. Sakulchaicharoen, D. M. O'Carroll, J. E. Herrera, Enhanced stability and dechlorination activity of pre-synthesis stabilized nanoscale FePd particles, *J. Contam. Hydrol.*, **118**, 117–127 (2010).

[5] P. Jiemvarangkul, W-x. Zhang, H-L. Lien, Enhanced transport of polyelectrolyte stabilized nanoscale zero-valent iron (nZVI) in porous media, *Chem. Eng. J.*, **170**, 482–491 (2011).

[6] R. A. Doong, Y. J. Lai, Dechlorination of tetrachloroethylene by palladized iron in the presence of humic acid, *Water Res.*, **39** (11), 2309–2318 (2005).

[7] J. Quinn, C. Geiger, C. Clausen, K. Brooks, C. Coon, S. O'Hara, T. Krug, D. Major, W.S. Yoon, A. Gavaskar, T. Holdsworth, Field demonstration

of DNAPL dehalogenation using emulsified zero-valent iron, *Environ. Sci. Technol.,* **39**, 1309–1318 (2005).

[8] S. R. Kanel, R. R. Goswami, T. P. Clement, M. O. Barnett, D. Zhao, Two dimensional transport characteristics of surface stabilized zero-valent iron nanoparticles in porous media, *Environ. Sci. Technol.*, **42** (3), 896–900 (2008).

[9] C. M. Cirtiu, T. Raychoudhury, S. Ghosal, A. Moores, Systematic comparison of the size, surface characteristics and colloidal stability of zero valent iron nanoparticles pre-and post-grafted with common polymers, *Colloid Surface A.*, **390**, 95–104 (2011).

[10] X. Qui, Z. Fang, X. Yan, W. Cheng, K. Lin, Chemical stability and toxicity of nanoscale zero-valent iron in the remediation of chromium-contaminated watershed, *Chem. Eng. J.*, **220**, 61–66 (2013).

[11] J. Fattison, S. Ghoshal, N. Tufenkji, Deposition of carboxymethyl cellulose-coated zero-valent iron nanoparticles onto silica: Roles of solution chemistry and organic molecules, *Langmuir*, **26** (15),12832–12840 (2010).

[12] F. He, D. Zhao, Preparation and characterization of a new class of starch-stabilized bimetallic nanoparticles for degradation of chlorinated hydrocarbons in water, *Environ. Sci. Technol.*, **39** (9) 3314–3320 (2005).

[13] H. M. Santos, J. L. Capelo, Trends in ultrasonic-based equipment for analytical sample treatment, *Talanta*, **73**, 795–802 (2007).

[14] Y. S. Ho, Review of second-order models for adsorption systems, *J. Hazard. Mater.*, **B136**, 681–689 (2006).

[15] G. Fritz, V. Schadler, N. Willenbacher, N. J. Wagner, Electrosteric stabilization of colloidal dispersions, *Langmuir*, 18, 6381–6390 (2002).

[16] T. Phenrat, N. Saleh, K. Sirk, H. J. Kim, R. D. Tilton, G. V. Lowry, Stabilization of aqueous nanoscale zerovalent iron dispersions by anionic polyelectrolytes: adsorbed anionic polyelectrolyte layer properties and their effect on aggregation and sedimentation, *J. Nanopart. Res.*, 10 (5), 795–814 (2008).

[17] G. B. Deacon, R. J. Phillips, Relationship between the carbon-oxygen stretching frequencies of carboxylate complexes and the type of carboxylate, *Coordin. Chem. Rev.*, 33, 227 (1980).

[18] F. He, D. Zhao, J. Lui, C. B. Roberts, Stabilization of Fe-Pd nanoparticles with sodium carboxymethyl cellulose for enhances transport and dechlorination of trichloroethylene in soil and groundwater, *Ind. Eng. Chem. Res.*, 46, 29–34 (2007).

[19] Y. H. Lin, H. H. Tseng, M. Y. Wey, M. D. Lin, Characteristics of two types of stabilized nano zero valent iron and transport in porous media, *Environ. Sci. Technol.*, **408**, 2260–2267 (2010).

[20] Z. Delci, D. Shyamala, S. Karuna, A. Senthil, A. Thayumanavan, Enhancement of optical, thermal and hardness in KDP crystals by boron doping, *Int. J. Chem. Tech. Res.*, **4** (2), 816–826 (2012).

[21] G. Kataby, M. Cojocaru, R. Prozoro, A. Gedanken, Coating carboxylic acids on amorphous iron nanoparticles, *Langmuir*, **15** (5), 1703–1708 (1999).

[22] T. Belin, N. Guigue-Millot, T. Caillot, D. Aymes, J. C. Niepce, Influence of grain size, oxygen stoichiometry, and synthesis conditions on the γ-Fe_2O_3 vacancies ordering and lattice parameters, *J. Solid State Chem.*, **163**, 459–465 (2002).

[23] R. D. Waldron, Infrared spectra of ferrites, *Phys. Rev.*, **99** (6), 1727–1735 (1955).

[24] C. L. Lin, C. F. Lee, W. Y. Chiu, Preparation and properties of poly (acrylic acid) oligomer stabilized superparamagnetic ferrofluid, *J. Colloid Interf. Sci.*, **29**, 411–420 (2005).

[25] L. T. Cuba-Chiem, L. Huynh, J. Ralston, D. A. Beattie, In situ particle film ATR FTIR spectroscopy of carboxymethyl cellulose adsorption on talc: binding mechanism, pH effects, and adsorption kinetics, *Langmuir*, **24**, 8036–8044 (2008).

[26] F. He, D. Zhao, Manipulating the size and dispersibility of zerovalent iron nanoparticles by use of carboxymethyl cellulose stabilizers, *Environ. Sci. Technol.*, **41**, 6216–6221 (2007).

[27] L. Greenlee, S. A. Hooker, Development of stabilized zero valent iron nanoparticles, *Desalin. Water Treat.*, **37**, 114–121 (2012).

[28] M. Dickinson, T. B. Scott, The application of zero-valent iron nanoparticles for the remediation of a uranium-contaminated waste effluent, *J. Hazard. Mater.*, **178**, 171–179 (2012).

[29] B. Geng, Z. Jin, T. Li, X. Qi, Kinetics of hexavalent chromium removal from water by chitosan-Fe^0 nanoparticles, *Chemosphere*, **75**, 825–830 (2009).

[30] W. F. Wust, R. Kober, O. Schlicker, A. Dahmke, Combined zero-and first order kinetic model of the degradation of TCE and cis-DCE with commercial iron, *Environ. Sci. Technol.*, **33** (23), 4304–4309 (1999).

[31] M. Cissoko, Z. Zhang, J. Zhang, X. Xu, Removal of Cr(VI) from simulative contaminated groundwater by iron metal, *Process Saf. Environ.*, **87**, 395–400 (2009).

[32] L-n. Shi, X. Zhang, Z-l. Chen, Removal of Chromium(VI) from wastewater using bentonite-supported nanoscale zero-valent iron, *Water Res.*, **45**, 886–892 (2011).

[33] F. He, D. Zhao, Hydrodechlorination of trichloroethene using stabilized Fe-Pd nanoparti-

cles: reaction mechanism and effects of stabilizers, catalysts and reaction conditions, *Appl. Catal. B.*, **84** (3–4), 533–540 (2008).

[34] Y. H. Xu, D. Zhao, Reductive immobilization of chromate in water and soil by stabilized iron nanoparticles, *Water Res.*, **41** (10), 2101–2108 (2007).

[35] P. Mitra, D. Sarkar, S. Chakrabarti, B. K. Dutta, Reduction of hexa-valent chromium with zero-valent iron: batch kinetic studies and rate model, *Chem. Eng. J.*, **171**, 54–60 (2011).

[36] H. H. Uhlig, R. W. Revie, *Corrosion and Corrosion Control*, John Wiley, New York, 1985.